CALPHAD: Computer Coupling of Phase Diagrams and Thermochemistry 91 (2025) 102889

Contents lists available at ScienceDirect

Calphad

journal homepage: www.elsevier.com/locate/calphad

High-pressure, high-temperature CALPHAD modelling of Ir–Os–Pt system

Julien Garcia , Jean-Marc Joubert *

Univ Paris Est Creteil, CNRS, ICMPE, UMR 7182, 2 rue Henri Dunant, Thiais, 94320, France

ARTICLE INFO

Keywords:
Calphad
Model
EOS
DFT
Iridium
High pressure
Iridium–osmium–platinum

ABSTRACT

In this paper, we use the CALPHAD method to describe iridium at high pressure and high temperature, based on the Lu's model as revisited by Joubert et al. (*Calphad: Comput. Coupling Phase Diagrams Thermochem.*, 74 (2021) 102304). A comprehensive literature review allowed us to obtain the equation of state for both the solid and liquid phases of Ir. We optimised the ambient-pressure phase diagrams of the Ir–Os and Ir–Pt systems with the experimental data from the literature and calculations performed in this study The successful reproduction of high-pressure experimental data for these alloys for the binary Ir–Os system, suggests a reliable description of both pure elements. Consequently, we can propose, for the first time, an extrapolation of the Ir–Os–Pt ternary diagram based on the descriptions of the binary systems.

1. Introduction

We recently adapted Lu's model [1] for the Calphad description of materials at high pressure and high temperature in order to correct some of the problematic extrapolations [2]. The new model was successfully applied to the description of Pt, Os and the binary system [3]. We continue our systematic investigation of Platinum Group Metals at high pressure and high temperature in present work with the study of iridium. Combining this description with those of the previously described Os and Pt allows the constitution of a three-component high-pressure database after the modeling of the two binary Ir–Os and Ir–Pt at ambient pressure.

2. Modelling and calculation details

2.1. High pressure model

The model used to describe high-pressure phases is the one developed by Lu et al. [1]. In this high-pressure model, the Gibbs energy is expressed with an additional contribution describing the change in volume as a function of temperature and pressure.

$$G = G(T, P_0) + \int V(T, P)dP$$

In Lu's model, the pressure and temperature dependence of the molar volume is expressed in the following equation:

$$V(T,P) = \boldsymbol{V_C} E_1^{-1}\left[E_1\left(\frac{\boldsymbol{V_0}\exp(\boldsymbol{V_A})}{\boldsymbol{V_C}}\right)\right] + (P - P_0)\boldsymbol{V_k}\exp\left(\frac{-\boldsymbol{V_0}\exp(\boldsymbol{V_A})}{\boldsymbol{V_C}}\right)$$

This model, already implemented in Thermo-Calc, requires four parameters to be determined:

V_0 which represents the volume at $T = 0$ K and $P = 1$ bar
V_A is the integrated thermal expansion
V_C is related to the pressure dependence of the bulk modulus
V_K is the isothermal compressibility at $P = 1$ bar

However, as described in the literature, this model exhibits an anomaly with C_p and entropy, which become negative at high pressure. To address this issue, Joubert et al. [2] proposed introducing a cut-off pressure to the V_A and V_K parameters to limit the thermal expansion at high pressure that has been identified as the cause of the problem. This revised model has already been applied to the description of Pt [2], Os [3], the Os–Pt system [3], Cr [4] and Sn [5]. All the optimisations of parameters have been done using the module PARROT of Thermo-Calc. All the thermodynamic calculations are done using Thermo-Calc.

2.2. DFT calculations

The enthalpy of mixing in both *fcc* and *hcp* solid solutions were obtained with SQS [6] in the two binary systems Ir–Pt and Os–Ir. We used 16-atom supercells at five compositions [7,8].

Density Functional Theory (DFT) calculations were carried out using

* Corresponding author.
E-mail address: jean-marc.joubert@cnrs.fr (J.-M. Joubert).

https://doi.org/10.1016/j.calphad.2025.102889
Received 19 August 2025; Received in revised form 10 October 2025; Accepted 10 October 2025

Vienna Ab-initio Simulation Package (VASP) [9,10] with projector augmented waves [11] and PBEsol [12] exchange-correlation functional. A plane-wave cut-off of 800 eV and dense Monkhorst–Pack k-point grids [13] were used for both *fcc* and hcp phases. Total energies were converged to 10^{-6} eV, and structures were relaxed until forces were below 10^{-8} eV Å^{-1}.

3. Selection of data

The list of experimental data used for optimization is given in Table 1.

3.1. Iridium

Iridium, like all platinum group metals, has very low compressibility and a very high melting point at 2719 K [14]. Iridium has an *fcc* structure and does not undergo any allotropic transformation up to the melting point. Cerenius et al. [15] reportedly observed a 14-layer closed-packed phase transition at $P = 65$ GPa, but the latter has never been found experimentally by other authors.

3.1.1. *fcc* iridium

The molar volume and thermal expansion of *fcc* iridium as a function of temperature up to the melting point have been studied by many authors [16–32]. Arblaster [23] has meticulously studied the literature data and modelled them. These evaluated data will be used as experimental inputs for modeling the *fcc* phase of the system.

Numerous measurements of molar volume variation as a function of pressure at 300 K are also available [22,31,33–46]. All the data collected, measured by X-ray diffraction (XRD), show good consistency up to a pressure of $P = 10$ GPa. Thus, the values of Monteseguro et al. [41], Yusenko et al. [47] and Anzellini et al. [44] will be retained for the optimization, as they are the most recent data. At higher pressures, Marsh et al. [35], Mcqueen et al. [34] and Seagle et al. [42] have carried out shock wave measurements up to 300 GPa. This data is very useful, as they provide information on molar volume at much higher pressures. Although these quantities are derived from indirect measurements, they will be taken into account in our optimization. High-temperature compressibility measurements were recently carried out by Anzellini et al. [44] and are proving invaluable, as they are the only information we have at high temperature and pressure.

With regard to bulk modulus values, we observe some disparities in the results reported by different authors [15,38,41,43,44,48]. Indeed, the bulk moduli specified in these studies are not measured directly but are instead derived from measurements of molar volume as a function of pressure. Moreover, these measurements do not provide any information on how the bulk modulus varies with temperature or pressure. In contrast, theoretical studies on iridium are available in the literature [22,32,40,49,50]. Among these, three authors provide values for the variation of bulk modulus with temperature: Liang et al. [32], Ferah et al. [22], and Kumar et al. [40]. For all these studies, the value of the bulk modulus at $T = 300$ K has the same order of magnitude as those obtained experimentally. We have chosen to disregard Kumar's values due to unusual behaviour observed at high temperatures. The values from Liang et al. and Ferah et al. are more appropriate. Since Liang's data includes information at higher temperatures, this will be used for the optimization.

3.1.2. Liquid iridium

Due to the high melting point, data for the liquid phase are less abundant.

Several authors have reported measurements of molar volume variation as a function of temperature [21,25,51–55]. In the same way as for the solid phase, Arblaster [53] has carried an assessment of the molar volume of the liquid phase up to $T = 3000$ K. This data will be taken into account for optimization. Wang et al. [55] has recently proposed new measurements of the density of liquid phases of different elements, these data will also be taken into account.

No data on the compressibility of the liquid phase has been found. On the other hand, melting points at different pressures are available [22,26,44,56]. Although data from Kulyamina et al. [26] are the result of calculations, the model has already proved its robustness for Os melting curve [3] and the corresponding data will be taken into account for the optimization. The experimental high-pressure point at 40 GPa given by Anzellini et al. [44] proves invaluable, as it gives us information on the linear character of the melting curve. This will also be taken into account in the optimization. Finally, Smirnov et al. [46] carried out calculations on the melting curve at very high pressure, giving us an indication of the potential behaviour of the system under these conditions.

3.2. Ir–Pt system

The Ir–Pt binary system was reviewed by Okamoto [57]. This system exhibits a significant miscibility gap in the *fcc* phase that has been investigated by various authors [58–61]. There is considerable uncertainty regarding the extent of this miscibility gap. Indeed, Raub et al. [61] and Tripathi et al. [60] conducted experimental studies and obtained significantly different results. To resolve this ambiguity, Yamabe et al. [59] studied the system and concluded that the diffusion of iridium and platinum was too slow. They proposed a miscibility gap determined by first-principles calculations, with a critical gap temperature of $T = 1573$ K. More recently, Zadesenets et al. [58] also investigated this issue and reportedly succeeded in achieving equilibrium, proposing a different miscibility gap with a much lower critical temperature of around 1050 K.

The authors have also measured lattice parameter at different concentrations [58–61]. Although there are slight discrepancies between the authors, the recent measurements by Zadesenets et al. [58] show a linear variation in the lattice parameter and thus compliance with Vegard's law.

Liquidus measurements at ambient pressure were carried out by Muller et al. [62] and represent the only information we have on the phase equilibrium between the solid and liquid phases.

Table 1
Selected data for optimization.

Phase	Data Type	Range	Reference	Experimental and/or modelling techniques
fcc Ir	*V-T* at $p = 1$ bar	0–2719 K	[23]	Assessment of experimental data
	α-T at $p = 1$ bar	0–2719 K	[23]	Assessment of experimental data
	V-p at $T = 300$ K	0–67 GPa	[43]	XRD
		0–34 GPa	[41]	XRD
		0–120 GPa	[44]	XRD
		0–300 GPa	[34]	Shock wave
		0–300 GPa	[35]	Shock wave
	B-T	0–2000 K	[32]	Calculation
	V-T-p	25–40 GPa	[44]	XRD
liquid Ir	*V-T*	2300–3000 K	[72]	Assessment of experimental data
		2200–2800 K	[55]	Electrostatic levitation
fcc-liq Ir	*P-T*	0–10 GPa	[56]	Calculation
		40 GPa	[44]	DRX
		0–100 GPa	[46]	Calculation
Ir-Pt	Enthalpy of mixing		This work	Calculation
	fcc-liquid		[62]	
Ir-Os	Enthalpy of mixing		This work	Calculation
	hcp-liquid		[65]	metallographic and pyrometric data
	fcc-liquid		[65]	metallographic and pyrometric data

No high-pressure or high-temperature data are available for this system.

3.3. Ir–Os system

The Ir–Os binary system was reviewed by Okamato [63]. It consists of a broad solubility of iridium in osmium *hcp* and osmium in iridium *fcc* separated by a two-phase *fcc* + *hcp* domain. The latter has been measured by several authors [64–66]. However, as the measurements by Vacher et al. [66] and Geballe et al. [38] are deemed to be out of equilibrium, only the values of Reiswig et al. [65] will be retained. The same authors, who carried out a complete study of the system, also provide us with information on the solidus and the presence of a peritectic invariant around 2873 K.

Various lattice parameter measurements are available for both *hcp* and *fcc* solid solutions [66–69].

Finally, Yusenko et al. measured compressibility and volume change as a function of temperature at different compositions [47,70]. They have also proposed a model of the Ir–Os system [71], which we will discuss in this article.

Finally, no phase equilibrium or compressibility data are available in the literature for the Ir–Os–Pt ternary system.

4. Modeling

4.1. Iridium at HP and HT

4.1.1. Solid phase

The data set selected for optimization was described in the previous section.

Thus, the parameters V_0 and V_A were determined from the molar volume values as a function of temperature and thermal expansion from Arblaster [23]. Concerning compressibility, the parameters V_c and V_K were found by DFT calculations of the bulk modulus as a function of temperature and various measurements of molar volume variation as a function of pressure. Finally, we adjusted the cut-off pressures of the model to reproduce the HP (high-pressure), HT (high-temperature) data given by Anzellini et al. [44] using values of $P_{cut} = 10^9$ Pa and $P'_{cut} = 10^{12}$ Pa.

4.1.2. Liquid phase

Concerning the liquid phase, as previously mentioned, the available data are much less. Since we have no information on the compressibility of the liquid phase, we have initially given this phase the same compressibility values V_c and V_K as the solid phase *fcc*. Then, we have optimised these parameters from the melting point dependence as a function of pressure.

The molar volume at 0 K of the liquid phase and the parameter V_A were determined from Kaptay et al. [25]. However, given the limited amount of data, in addition to optimizing the Arblaster [53] and Wang et al. [55] values, we decided to add an additional term to the liquid phase parameter V_A, to ensure that the liquid phase retains the same curvature as the *fcc* phase.

The agreement between data and the model is shown in Figs. 1–5. All the data was correctly described. The plot of thermal expansions at different pressures in Fig. 1(b) shows the influence of cut-off pressures.

4.2. Iridium–platinum system

4.2.1. Ir–Pt at ambient pressure

The interaction parameters of the *fcc* solid solution (Ir,Pt) cannot be determined from the experimental data given by various authors due to the excessive dispersion and the lack of information as to whether the various samples synthesised are in equilibrium or not [59]. In order to define the interaction parameters of the *fcc* phase, we performed SQS and DFT calculations giving us the enthalpies of mixing between these two elements at different compositions and we neglected the excess entropy of mixing. The critical temperature of the gap calculated in this way agrees well with that obtained by Raub et al. [59]. The liquid interaction parameters (Ir,Pt) were determined using the liquidus measurements of Muller et al. [34].

Although these elements are both *fcc*, a description of the interaction in the *hcp* phase is necessary if we want to calculate the ternary diagram including Os, which is *hcp*. As with the *fcc* phase, we have determined the interaction parameters of the *hcp* solid solution (Ir,Pt) using enthalpies of mixing obtained by SQS calculations.

4.2.2. Ir–Pt at high pressure

High-pressure platinum has already been modelled by Joubert et al. [2]. Corresponding parameters will therefore be used to model this system at high-pressure.

No compressibility data is available for this system. The various lattice parameter measurements carried out by different authors at ambient pressure show a linear variation in the lattice parameter, which means that no interaction parameter is required to define the V_A parameter. This implies that there will be no modification of the miscibility gap as a function or pressure. SQS-DFT data has been added for comparison. The DFT values obtained within the GGA always over-

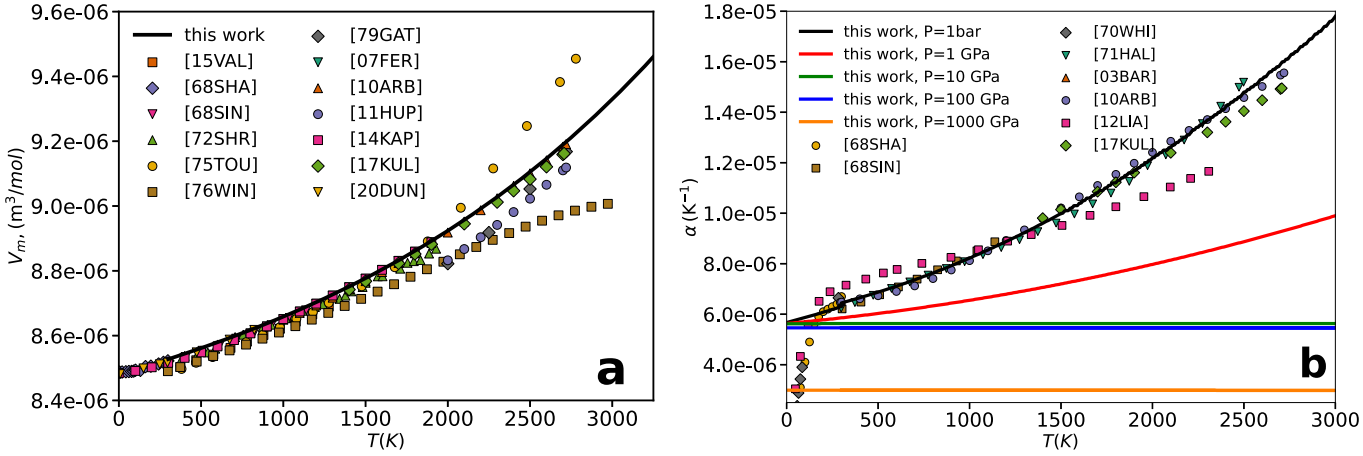

Fig. 1. (a) Molar volume of *fcc* Ir at $P = 1$ bar as a function of temperature. The experimental data are from [15VAL] [16], [68SHA] [17], [68SIN] [18], [72SHR] [19], [75TOU] [28], [76WIN] [20], [79GAT] [21], [07FER] [22], [10ARB] [23], [11HUP] [24], [14KAP] [25], [17KUL] [26] and [20DUN] [27]. (b) Linear thermal expansion of *fcc* Ir at $P = 1$ bar as a function of temperature. The experimental data are from [68SHA] [17], [68SIN] [18], [70WHI] [29], [71HAL] [30], [03BAR] [31], [10ARB] [23], [12LIA] [32] and [17KUL] [26].

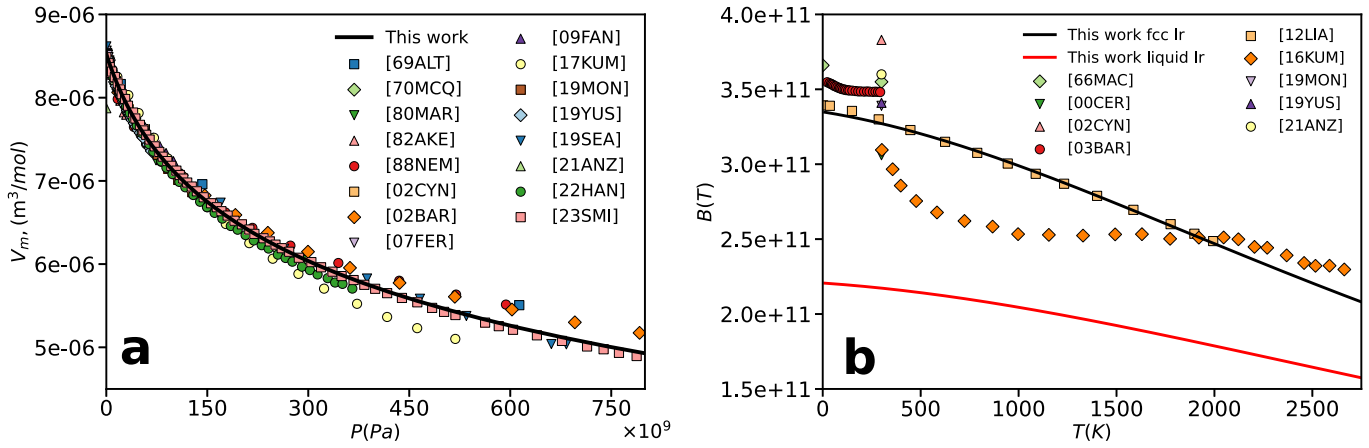

Fig. 2. (a) Molar volume of *fcc* Ir as a function of pressure à $T = 300$K. The experimental data are from [69ALT] [33], [70MCQ] [34], [80MAR] [35], [82AKE] [36], [88NEM] [37], [02CYN] [38], [02BAR] [31], [07FER] [22], [09FAN] [39], [17KUM] [40], [19MON] [41], [19YUS] [43], [19SEA] [42], [21ANZ] [44], [22HAN] [45] and [23SMI] [46]. (b) Bulk modulus of *fcc* Ir as a function of temperature. The experimental data are from [66MAC] [48], [00CER] [15], [02CYN] [38], [03BAR] [31], [12LIA] [32], [16KUM] [40], [19MON] [41], [19YUS] [43] and [21ANZ] [44].

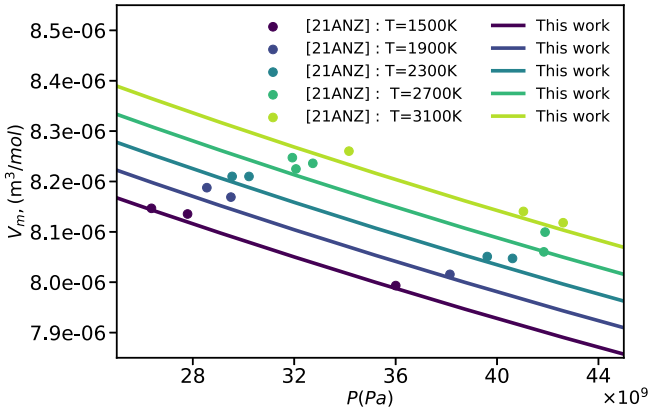

Fig. 3. Molar volume of *fcc* Ir as a function of pressure at different temperatures. The experimental data is from [21ANZ] [44].

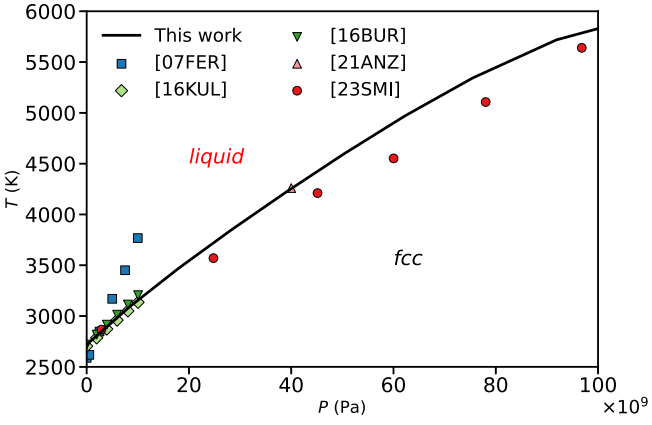

Fig. 4. Melting curve of Ir. The experimental data are from [07FER] [22], [16KUL] [26], [16BUR] [56], [21ANZ] [44] and [23SMI] [46].

estimate the lattice parameters but the linear behavior observed experimentally is confirmed. Calculation of the system at high pressure can be performed without any additional parameter. The dependence of the interaction parameters as a function of pressure is considered to be negligible as was observed previously in Os–Pt system [3].

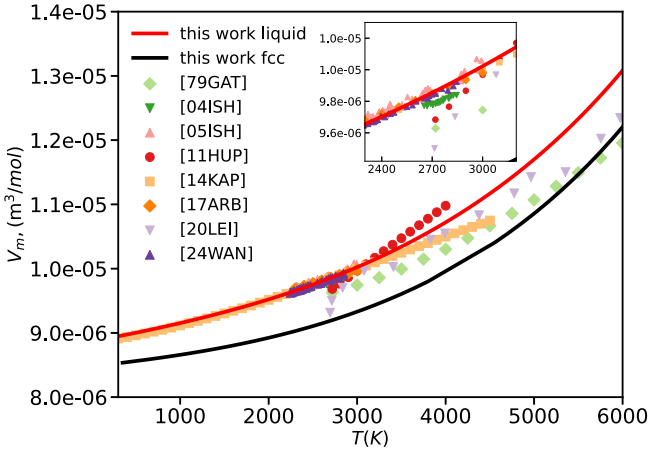

Fig. 5. Molar volume of *liquid* Ir as a function of temperature. The experimental data are from [79GAT] [21], [04ISH] [51], [05ISH] [52], [11HUP] [24], [14KAP] [25], [17ARB] [72], [20LEI] [54] and [24WAN] [55].

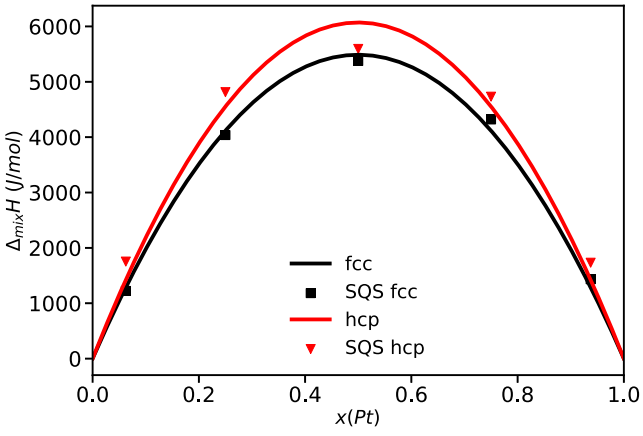

Fig. 6. Enthalpies of mixing of the *fcc* and *hcp* phases in the Ir–Pt system. The SQS calculation is from this work.

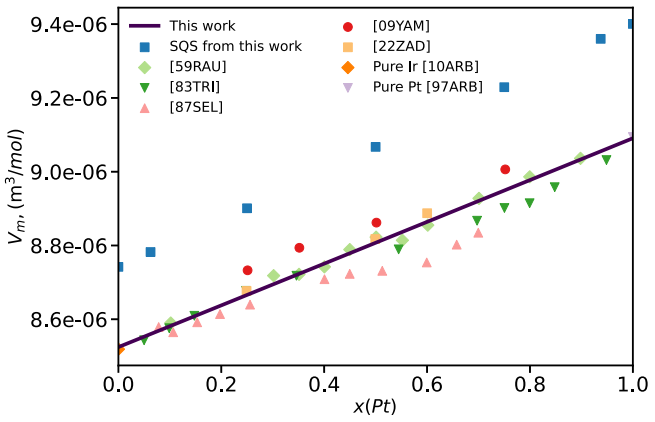

Fig. 7. Molar volume of the Ir–Pt *fcc* phase at 300 K and ambient pressure. The experimental data are from [59RAUB] [73], [83TRI] [60], [87SEL] [74], [09YAM] [59] and [22ZAD] [58].

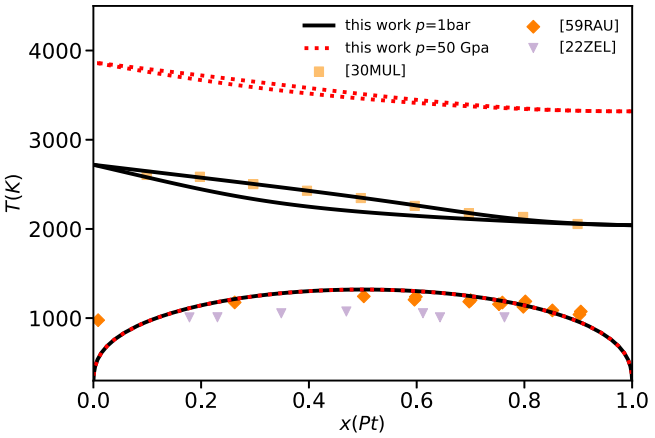

Fig. 8. Calculated phase diagram of the Ir–Pt system at $P = 1$ bar and $P = 50$ GPa. The experimental data at $P = 1$ bar are from [30MUL] [62], [59RAU] [73] et [22ZAD] [58].

The model and experimental data for Ir–Pt system are shown in Figs. 6–8.

4.3. Iridium–osmium system

4.3.1. Metastable phases hcp Ir and fcc Os

In order to be able to describe the compressibility data for the Ir–Os system, a description of the HP parameters of the metastable phase *hcp* Ir is required. To determine the parameter V_0 of the *hcp* Ir phase, we decided to base ourselves on measurements of molar volume as a function of composition for the *hcp* phase à T = 300 K. In the solution domain, experimental data shows that the composition dependence is linear, as observed also by the SQS-DFT calculations, though with a significant shift, as explained above. We extrapolated to pure *hcp* Ir from this experimental data obtaining a value of $V_m = 8.5473.10^{-6} m^3/mol$ for *hcp* Ir at 300 K as shown in Fig. 9. With regard to the other parameters, we assume that the metastable *hcp* phase behaves in the same way as the *fcc* phase, so we keep the same parameters as the *fcc* phase.

Joubert et al. [3] provide the molar volume V_0 of the *fcc* phase of

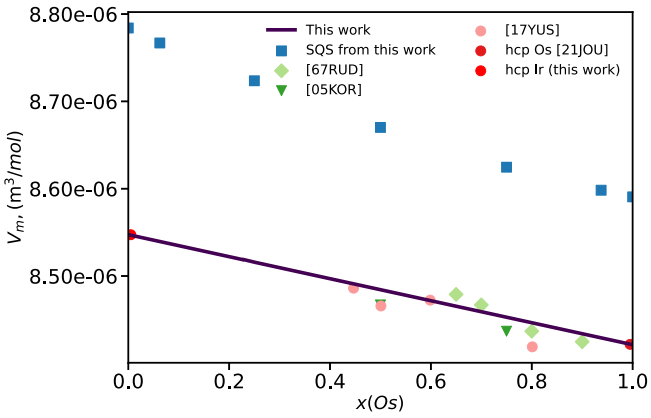

Fig. 9. Molar volume of the Ir–Os *hcp* phase at $T = 300$ K. The experimental data are from [67RUD] [68], [05KOR] [67],[17YUS] [47] and [JOU21] [3].

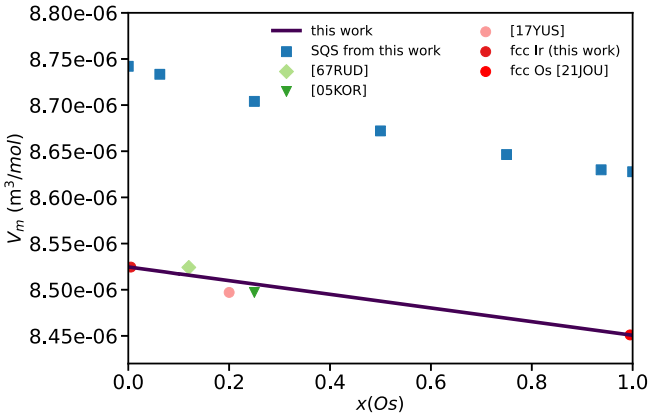

Fig. 10. Molar volume of the Ir–Os *fcc* phase at $T = 300$ K. The experimental data are from [67RUD] [68], [05KOR] [67], [17YUS] [47] and [JOU21] [3].

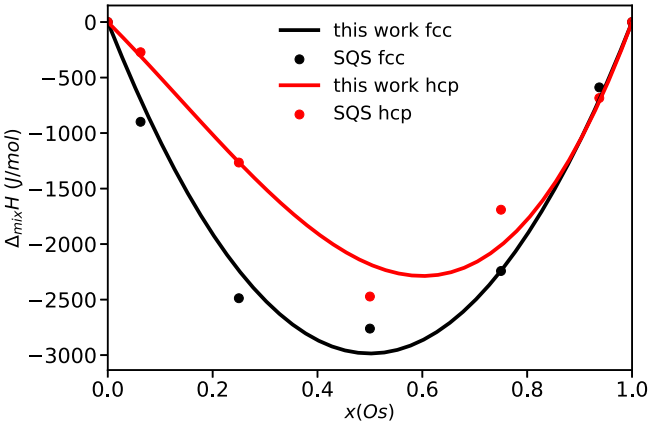

Fig. 11. Enthalpies of mixing in the Ir–Os *fcc* and *hcp* phases. The SQS calculation is from this work.

osmium, which enables the calculation of the variation of molar volume as a function of composition for the *fcc* phase. As observed for the *hcp* phase, this variation is fairly linear (Fig. 10).

4.3.2. Ir–Os at ambient pressure

Regarding the modelling of the Ir–Os phase diagram at ambient pressure, we observe a discrepancy between the values calculated using SQS and the phase diagram experimental data. It is not possible to reconcile both the phase equilibrium data from Reiswing et al. [65] and the enthalpy of mixing calculations (see below the previous thermodynamic optimization by Yusenko et al. [71]). We therefore have two options: the first is to ignore the SQS calculations and rely solely on the experimental measurements; the second is to assume that the measurements are out of equilibrium and optimise only the SQS results. Considering the low diffusion of atoms as in the Ir–Pt system [59], the experimental data available may not be completely in equilibrium at lower temperature. It is also difficult to imagine that the solubility limits do not change as a function of temperature as shown by experiments. Finally, we have already been able to describe the Ir–Pt system satisfactorily using calculated data. For these reasons, we have decided to optimise the SQS data rather than the phase equilibrium data for the interaction parameter of *hcp* and *fcc* phases (Fig. 11). As always done for solutions, we do not consider any temperature dependence of the enthalpy of mixing (Neumann-Kopp), so that the 0 K calculation can be safely used at high temperature. For the liquid phase, we have optimised Reiswing's experimental solidus data [65].

The modelled phase diagram is shown in Fig. 12.

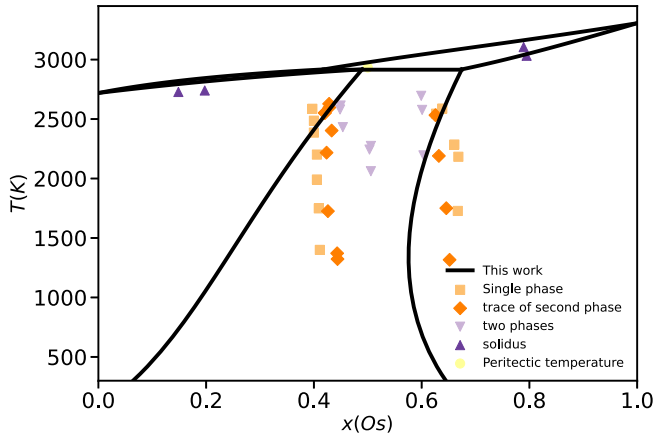

Fig. 12. Calculated phase diagram of the Ir–Os system at $P = 1$ bar from SQS calculation. The experimental data are from [64REI] [65].

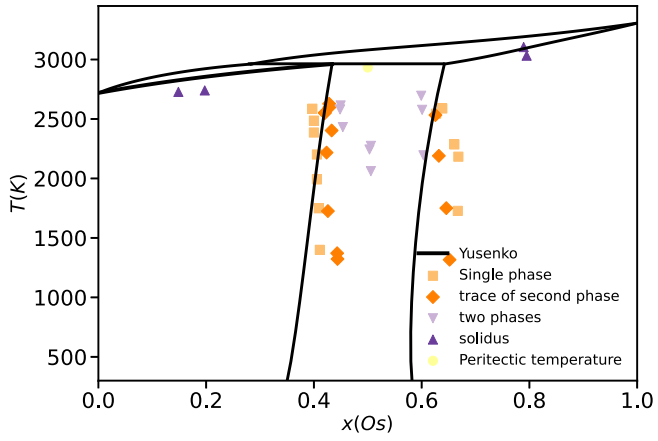

Fig. 13. Calculated phase diagram of the Ir–Os system at $P = 1$ bar with the parameters from Yusenko et al. [71]. The experimental data are from [64REI] [65].

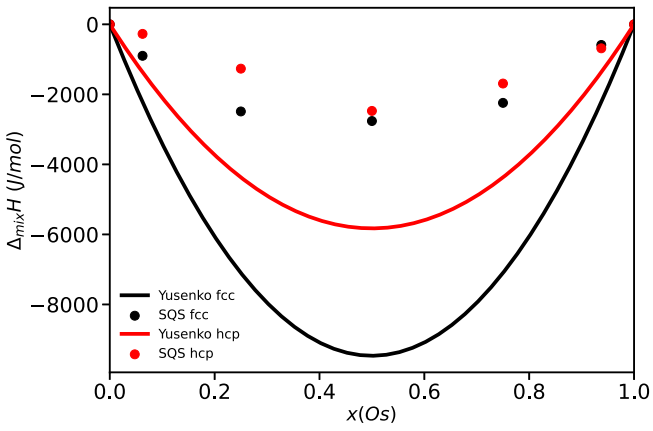

Fig. 14. Enthalpies of mixing in the Ir–Os *fcc* and *hcp* phases from Yusenko et al. [71] compared to the SQS calculation is from this work.

4.3.3. Previous modelling

In a recent study of the Ir–Os–Ru system, Yusenko et al. [71] also proposed an ambient pressure model of the Ir–Os system. Where we chose to optimise the calculated enthalpy of mixing data, the latter chose to optimise the experimental data. The phase diagram calculated with these parameters satisfactorily describes the experimental phase diagram (Fig. 13) but could not account the present SQS calculations (Fig. 14).

4.3.4. Ir–Os at high pressure

All the high-pressure parameters for Os were determined previously by Joubert et al. [3].

Remakedly, most of the measurements of variations in molar volume as a function of temperature and pressure carried out by Yusenko et al. [47,70] at different compositions could be reproduced without optimizing interactions parameters (Figs. 15–16), with the exception of the data shown in Fig. 17. These experimental points measured at HP and HT cannot be reproduced using our model. Measurements at HP and HT are very difficult to carry out and are much less accurate [75], so we discarded the measurements in Fig. 15 and kept only the measurements in Figs. 15 and 16.

We can therefore propose a high-pressure phase diagram for the Ir–Os system (Fig. 18).

The presence of the *fcc* Os phase at high temperatures results from a poor description of the pure elements in the SGTE database, as previously discussed by Joubert [2]. This artifact should not be considered in the present study.

Regarding the two-phase *hcp* + *fcc* domain, we observe that it is only

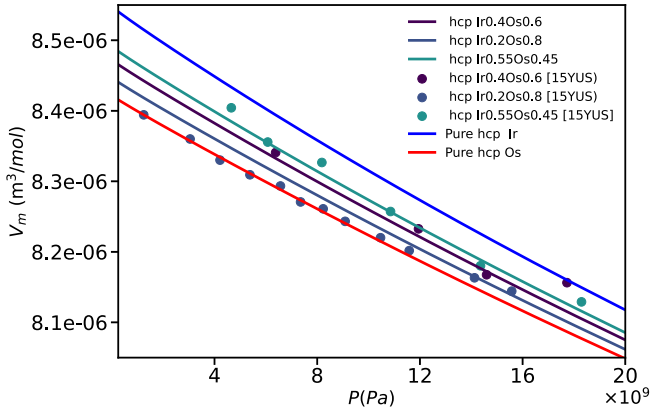

Fig. 15. Molar volume as a function of pressure of *hcp*-$Ir_{20}Os_{80}$, *hcp*-$Ir_{60}Os_{40}$ and *hcp*-$Ir_{55}Os_{45}$ at $T = 300$K. The experimental data are from [15YUS] [70].

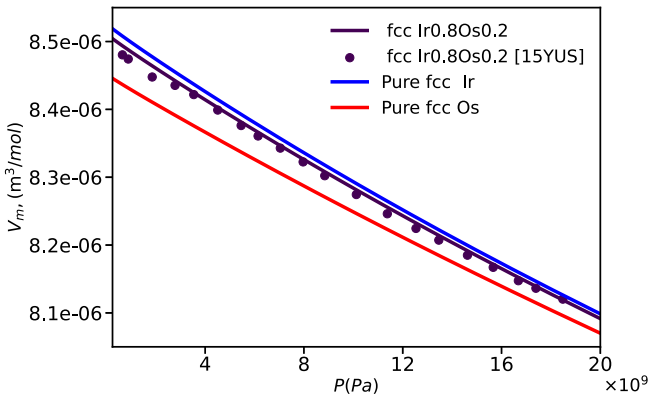

Fig. 16. Molar volume as a function of pressure of *fcc*-$Ir_{80}Os_{20}$ at $T = 300$K. The experimental data are from [15YUS] [70].

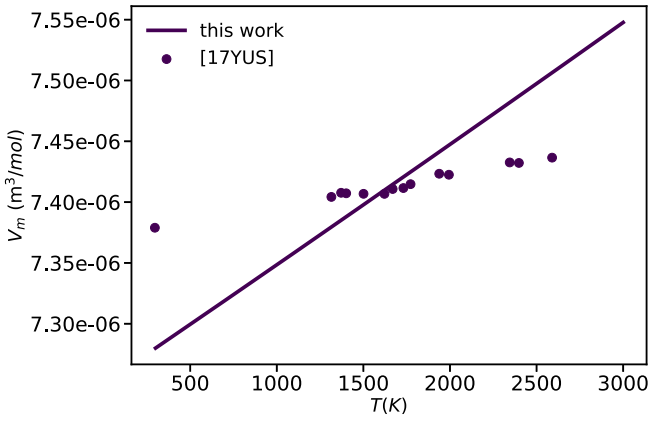

Fig. 17. Molar volume as a function of temperature of hcp-$Ir_{55}Os_{45}$ at $P = 80$ GPa. The experimental data are from [17YUS] [47].

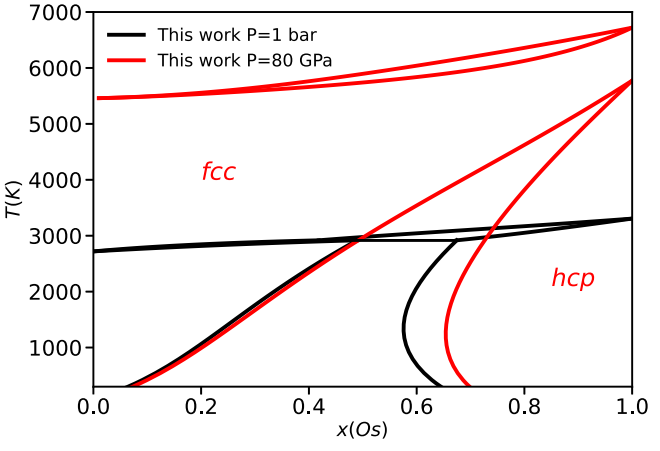

Fig. 18. High pressure calculated phase diagram of the Ir–Os system at $P = 80$ GPa.

marginally affected by the increase of pressure. This finding does not align with the prediction of Yusenko et al. [47], who forecast a shift of the two-phase domain toward the Iridium-rich side with increasing pressure. This discrepancy occurs even though the experimental data have been adequately described by the model parameters.

5. Ir–Os–Pt system

The list of optimization parameters is given in Table 2.
Based on the modelling of iridium, platinum, and osmium, as well as

Table 2
Ir–Os–Pt system parameters.

Phase	Parameter	Value (p in Pa, L in J/mol, V_0 and V_C in m^3/mol, V_K in Pa^{-1})	Ref
	P_{cut}	1 x 10^9	This work
	P^{Ir}_{cut}	1 x 10^{12}	This work
	P^{Os}_{cut}	1.6667 x 10^{11}	[3]
	P^{Pt}_{cut}	1.1051 x 10^{11}	[1]
fcc	${}^0L_{Ir,Pt}$	2.1846 x 10^4	This work
	${}^0L_{Os,Pt}$	2.2965 x 10^4+ 1.8241 x T	[3]
	${}^1L_{Os,Pt}$	−1.1715 x 10^4 + 6.39 x T	[3]
	${}^0L_{Ir,Os}$	−1.1941 x 10^4 + 9.526 x T	This work
	${}^1L_{Ir,Os}$		
	V^{Ir}_0	8.48 x 10^{-6}	This work
	V^{Ir}_A	1.7010 x 10^{-5} T $\exp\left(-\frac{P}{P^{Ir}_{cut}}\right)$ +2.8480x10^{-9} T^2 $\exp\left(-\frac{P}{P_{cut}}\right)$ + 6.8476x 10^{-13} T^3 $\exp\left(-\frac{P}{P_{cut}}\right)$	This work
	V^{Ir}_C	1.5333 x 10^{-6}	This work
	V^{Ir}_K	2.9855 x 10^{-12} + 1.8537x $10^{-16}T$ $\exp\left(-\frac{P}{P_{cut}}\right)$ + 1.7326x10^{-19} T^2 $\exp\left(-\frac{P}{P_{cut}}\right)$	This work
	V^{Os}_0	8.4152 x 10^{-6}	[3]
	V^{Os}_A	1.3621x 10^{-5} T $\exp\left(-\frac{P}{P^{Os}_{cut}}\right)$ + 2.3291x10^{-9} T^2 $\exp\left(-\frac{P}{P_{cut}}\right)$	[3]
	V^{Os}_C	2.0069 10^{-6}	[3]
	V^{Os}_K	2.5044x 10^{-12} + 1.6 x$10^{-16}T$ $\exp\left(-\frac{P}{P_{cut}}\right)$+ 5.99 x 10^{-20} T^2 $\exp\left(-\frac{P}{P_{cut}}\right)$	[3]
	V^{Pt}_0	9.0204 x 10^{-6}	[1]
	V^{Pt}_A	2.5977x 10^{-5} T $\exp\left(-\frac{P}{P^{Pt}_{cut}}\right)$ + 1.3533x10^{-9} T^2 $\exp\left(-\frac{P}{P_{cut}}\right)$ + 1.2683x 10^{-12} T^3 $\exp\left(-\frac{P}{P_{cut}}\right)$	[1]
	V^{Pt}_C	1.6844x 10^{-6}	[1]
	V^{Pt}_K	3.6579 x 10^{-12}-1.0875 x 10^{-16} T $\exp\left(-\frac{P}{P_{cut}}\right)$ +5.6029 x 10^{-19} T^2 $\exp\left(-\frac{P}{P_{cut}}\right)$	[1]
hcp	${}^0L_{Ir,Pt}$	2.4285 x 10^4	This work
	${}^0L_{Os,Pt}$	5.2174 x 10^4	[3]
	${}^1L_{Os,Pt}$	−1.0342 x 10^4	[3]
	${}^0L_{Ir,Os}$	−8.7315 x 10^3 + 11.972 x T	This work
	${}^1L_{Ir,Os}$	3.9961 x 10^3	This work
	V^{Ir}_0	8.5 x 10^{-6}	This work
	V^{Ir}_A	1.7807 x 10^{-5} T $\exp\left(-\frac{P}{P^{Ir}_{cut}}\right)$ +2.1919 x10^{-9} T^2 $\exp\left(-\frac{P}{P_{cut}}\right)$ + 8.2622 x 10^{-13} T^3 $\exp\left(-\frac{P}{P_{cut}}\right)$	This work
	V^{Ir}_C	1.6497 x 10^{-6}	This work

(*continued on next page*)

Table 2 (*continued*)

Phase	Parameter	Value (p in Pa, L in J/mol, V_0 and V_C in m^3/mol, V_K in Pa^{-1})	Ref
	V_K^{Ir}	$2.9284 \times 10^{-12} + 3.0859 \times 10^{-16}\, T \exp\left(-\frac{P}{P_{cut}}\right) + 1.1838 \times 10^{-19}\, T^2 \exp\left(-\frac{P}{P_{cut}}\right)$	This work
	V_0^{Os}	8.3852×10^{-6}	[3]
	V_A^{Os}	$1.3621 \times 10^{-5}\, T \exp\left(-\frac{P}{P_{cut}^{Os}}\right) + 2.3291 \times 10^{-9}\, T^2 \exp\left(-\frac{P}{P_{cut}}\right)$	[3]
	V_C^{Os}	2.0069×10^{-6}	[3]
	V_K^{Os}	$2.4492 \times 10^{-12} + 1.60 \times 10^{-16}\, T \exp\left(-\frac{P}{P_{cut}}\right) 5.9999 \times 10^{-20}\, T^2 \exp\left(-\frac{P}{P_{cut}}\right)$	[3]
	V_0^{Pt}	9.0804×10^{-6}	[1]
	V_A^{Pt}	$2.5977 \times 10^{-5}\, T \exp\left(-\frac{P}{P_{cut}^{Pt}}\right) + 1.3533 \times 10^{-9}\, T^2 \exp\left(-\frac{P}{P_{cut}}\right) + 1.2683 \times 10^{-12}\, T^3 \exp\left(-\frac{P}{P_{cut}}\right)$	[1]
	V_C^{Pt}	1.6844×10^{-6}	[1]
	V_K^{Pt}	$3.7825 \times 10^{-12} - 1.0875 \times 10^{-16}\, T \exp\left(-\frac{P}{P_{cut}}\right) + 5.6029 \times 10^{-19}\, T^2 \exp\left(-\frac{P}{P_{cut}}\right)$	[1]
Liquid	${}^0L_{Ir,Pt}$	1.3994×10^4	This work
	${}^0L_{OS,Pt}$	2.4344×10^4	[3]
	${}^0L_{Ir,Os}$	2.1242×10^4	This work
	V_0^{Ir}	8.866×10^{-6}	This work
	V_A^{Ir}	$2.9372 \times 10^{-5}\, T \exp\left(-\frac{P}{P_{cut}^{Ir}}\right) + 1.7476 \times 10^{-9}\, T^2 \exp\left(-\frac{P}{P_{cut}}\right) + 6.9476 \times 10^{-13}\, T^3 \exp\left(-\frac{P}{P_{cut}}\right)$	This work
	V_C^{Ir}	2.3335×10^{-6}	This work
	V_K^{Ir}	$4.5307 \times 10^{-12} + 1.8557 \times 10^{-16}\, T \exp\left(-\frac{P}{P_{cut}}\right) + 1.7325 \times 10^{-19}\, T^2 \exp\left(-\frac{P}{P_{cut}}\right)$	This work
	V_0^{Os}	9.1×10^{-6}	[3]
	V_A^{Os}	$1.7 \times 10^{-5}\, T \exp\left(-\frac{P}{P_{cut}^{Os}}\right) + 2.3291 \times 10^{-9}\, T^2 \exp\left(-\frac{P}{P_{cut}}\right)$	[3]
	V_C^{Os}	2.0069×10^{-6}	[3]
	V_K^{Os}	$2.4535 \times 10^{-12} + 1.60 \times 10^{-16}\, T \exp\left(-\frac{P}{P_{cut}}\right) + 5.99 \times 10^{-20}\, T^2 \exp\left(-\frac{P}{P_{cut}}\right)$	[3]
	V_0^{Pt}	9.4686×10^{-6}	[1]
	V_A^{Pt}	$2.9546 \times 10^{-5}\, T \exp\left(-\frac{P}{P_{cut}^{Pt}}\right) + 1.3976 \times 10^{-12}\, T^3 \exp\left(-\frac{P}{P_{cut}}\right)$	[1]
	V_C^{Pt}	1.4409×10^{-6}	[1]
	V_K^{Pt}	$5.0 \times 10^{-12} + 6.2265 \times 10^{-19}\, T^2 \exp\left(-\frac{P}{P_{cut}}\right)$	[1]

their underlying binary systems, it is now possible to predict the phase diagram of the Ir–Os–Pt ternary system at ambient and at high pressure (see Figs. 19 and 20). No experimental or theoretical data are available in the literature for this ternary system to verify the accuracy, so the isothermal section should be considered as tentative. However, the high-pressure experimental data for the binary systems have been reproduced without the need for interaction parameters, which supports the reliability of the ternary system projection.

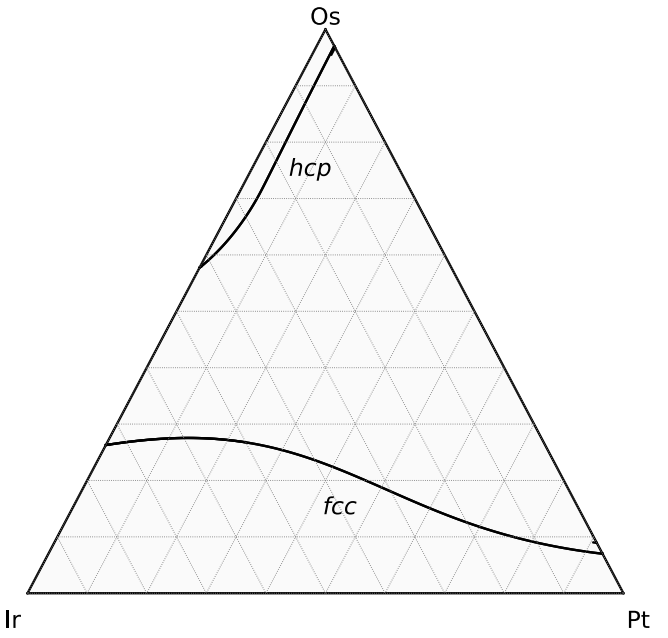

Fig. 19. Calculated phase diagram of the Ir–Os–Pt at $P = 1$ bar and $T = 1500$K.

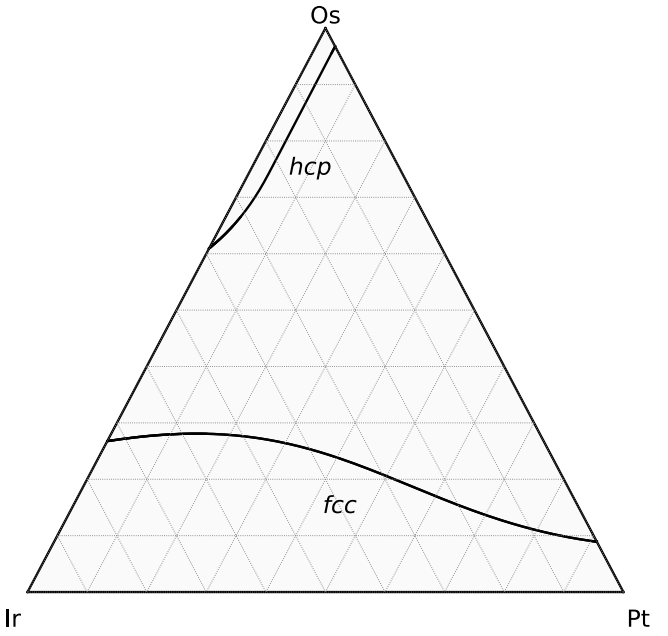

Fig. 20. Calculated phase diagram of the Ir–Os–Pt at $P = 100$ GPa and $T = 1500$K.

6. Conclusion

Pure iridium was accurately described at high pressure and high temperature using the revised Lu's model. The Ir–Os and Ir–Pt binary systems were also accurately described based on both experimental and calculated data. The successful description of compressibility and thermal expansion measurements confirms the robustness of the model for high-pressure binary systems. Therefore, based on these three binary system descriptions, we were able to predict and propose, for the first time, the Ir–Os–Pt ternary phase diagram at both ambient and high pressures.

CRediT authorship contribution statement

Julien Garcia: Investigation, Formal analysis, Data curation. **Jean-Marc Joubert:** Writing – review & editing, Validation, Supervision, Project administration, Funding acquisition.

Declaration of competing interest

The authors declare that they have no known competing financial interests or personal relationships that could have appeared to influence the work reported in this paper.

Acknowledgement

The authors thank Jean-Claude Crivello for providing us with the SQS calculations.

Appendix A. Supplementary data

Supplementary data to this article can be found online at https://doi.org/10.1016/j.calphad.2025.102889.

Data availability

Data will be made available on request.

References

[1] X.-G. Lu, M. Selleby, B. Sundman, Implementation of a new model for pressure dependence of condensed phases in thermo-calc, Computer Coupling of Phase Diagrams and Thermochem. 29 (2005) 49–55, https://doi.org/10.1016/j.calphad.2005.04.001.
[2] J.-M. Joubert, J.-M. Crivello, Modification of Lu's (2005) high pressure model for improved high pressure/high temperature extrapolations. Part I: modeling of platinum at high pressure/high temperature, Calphad (2021), https://doi.org/10.1016/j.calphad.2021.102304.
[3] J.-M. Joubert, J.-C. Crivello, K.V. Yusenko, Modification of Lu's (2005) high pressure model for improved high pressure/high temperature extrapolations. Part II: modeling of osmium–platinum system at high pressure/high temperature, Calphad 74 (2021) 102311, https://doi.org/10.1016/j.calphad.2021.102311.
[4] M. Dottor, J.-C. Crivello, J.-M. Joubert, Thermodynamic modeling of Cr and Cr–H systems up to high temperatures and high pressures, Int. J. Hydrogen Energy 47 (2022) 23293–23309, https://doi.org/10.1016/j.ijhydene.2022.04.245.
[5] G. Deffrennes, P. Faure, F. Bottin, J.-M. Joubert, B. Oudot, Tin (sn) at high pressure: review, X-ray diffraction, DFT calculations, and gibbs energy modeling, J. Alloys Compd. 919 (2022) 165675, https://doi.org/10.1016/j.jallcom.2022.165675.
[6] A. Zunger, S.-H. Wei, L.G. Ferreira, J.E. Bernard, Special quasirandom structures, Phys. Rev. Lett. 65 (1990) 353–356, https://doi.org/10.1103/PhysRevLett.65.353.
[7] C. Wolverton, Crystal structure and stability of complex precipitate phases in Al-Cu-Mg-(Si) and al-zn-mg alloys, Acta Mater. 49 (2001) 3129–3142, https://doi.org/10.1016/S1359-6454(01)00229-4.
[8] D. Shin, R. Arróyave, Z.-K. Liu, A. Van de Walle, Thermodynamic properties of binary hcp solution phases from special quasirandom structures, Phys. Rev. B74 (2006) 024204, https://doi.org/10.1103/PhysRevB.74.024204.
[9] G. Kresse, J. Furthmüller, Efficiency of ab-initio total energy calculations for metals and semiconductors using a plane-wave basis set, Comput. Mater. Sci. 6 (1996) 15–50, https://doi.org/10.1016/0927-0256(96)00008-0.
[10] G. Kresse, D. Joubert, From ultrasoft pseudopotentials to the projector augmented-wave method, Phys. Rev. B 59 (1999) 1758–1775.
[11] P.E. Blöchl, Projector augmented-wave method, Phys. Rev. B 50 (1994) 17953–17979, https://doi.org/10.1103/PhysRevB.50.17953.
[12] G.I. Csonka, J.P. Perdew, A. Ruzsinszky, P.H.T. Philipsen, S. Lebègue, J. Paier, O. A. Vydrov, J.G. Angyan, Assessing the performance of recent density functionals for bulk solids, Phys. Rev. B79 (2009) 155107, https://doi.org/10.1103/PhysRevB.79.155107.
[13] H.J. Monkhorst, J.D. Pack, Special points for Brillouin-zone integrations, Phys. Rev. B 13 (1976) 5188–5192, https://doi.org/10.1103/PhysRevB.13.5188.
[14] R.E. Bedford, G. Bonnier, H. Maas, F. Pavese, Recommended values of temperature on the international temperature scale of 1990 for a selected set of secondary reference points, Metrologia 33 (1996) 133, https://doi.org/10.1088/0026-1394/33/2/3.
[15] Y. Cerenius, L. Dubrovinsky, Compressibility measurements on iridium, J. Alloys Compd. 306 (2000) 26–29, https://doi.org/10.1016/s0925-8388(00)00767-2.
[16] S. Valentiner, J. Wallot, Über die Abhängigkeit des Ausdehnungskoeffizienten fester Körper von der Temperatur, Ann. Phys. 351 (1915) 837–867, https://doi.org/10.1002/andp.19153510609.
[17] H.F. Shaake, Thermal expansion of iridium from 4.2 to 300°K, J. Less Common. Met. 15 (1968) 103–105, https://doi.org/10.1016/0022-5088(68)90012-X.
[18] H.P. Singh, Determination of thermal expansion of germanium, rhodium, and iridium by X-rays, Acta Crystallogr. 24 (1968) 469–471, https://doi.org/10.1107/S056773946800094X.
[19] R.H. Schroeder, N. Schmitz-Pranghe, R. Kohlhaas, Experimentelle Bestimmung der Gitterparameter der Glatinmetalle im Gemperaturbereich von - 190 bis 1709°C, Z. Metallkd. 63 (1972) 12–16, https://doi.org/10.1515/ijmr-1972-630103.
[20] R.T. Wimber, High-temperature thermal expansion of iridium (revised results), J. Appl. Phys. 47 (1976), https://doi.org/10.1063/1.322479, 5115-5115.
[21] G.R. Gathers, J.W. Shaner, R.S. Hixson, D.A. Young, Very high temperature thermophysical properties of solid and liquid vanadium and iridium, High. Temp. - High. Press. 11 (1979) 653–668.
[22] G. Ferah, K. Colakoglu, Y. Ciftci, S. Ozgen, S. Kazanc, A molecular dynamics study on iridium, Open Phys. 5 (2007) 207–220, https://doi.org/10.2478/s11534-007-0011-z.
[23] J.W. Arblaster, Crystallographic properties of iridium, Platinum Met. Rev. 54 (2010) 99–102, https://doi.org/10.1595/147106710X493124.
[24] T. Hüpf, G. Pottlacher, Thermal expansion of Ir, Pd, Pt, and V obained in fast pluse-heating experiments, High. Temp. - High. Press. 40 (2011) 271–279.
[25] G. Kaptay, Approximated equations for molar volumes of pure solid fcc metals and their liquids from zero kelvin to above their melting points at standard pressure, J. Mater. Sci. 50 (2014), https://doi.org/10.1007/s10853-014-8627-z, 678-587.
[26] E.Y. Kulyamina, V.Y. Zitserman, L.R. Fokin, Calculating the melting curves by the thermodynamic data matching method: platinum-group refractory metals (Ru, Os, and Ir), Tech. Phys. 62 (2017) 68–74, https://doi.org/10.1134/S1063784217010145.
[27] D.H. Moseley, S.J. Thébaud, L.R. Lindsay, Y. Cheng, D.L. Abernathy, M.E. Manley, R.P. Hermann, Temperature-dependent lattice dynamics in iridium, Phys. Rev. Mater. 4 (2020) 113608, https://doi.org/10.1103/PhysRevMaterials.4.113608.
[28] Y.S.K. Touloukian, , R. K., R.E. Taylor, P.D. Desai, Thermophysical Properties of Matter, 1975.
[29] G.K. White, A.T. Pawliwicz, Thermal expansion of rhodium, iridium, and palladium at low temperatures, J. Low Temp. Phys. 2 (1970) 631–639, https://doi.org/10.1007/BF00628279.
[30] J.J. Halvorson, R.T. Winber, Thermal expansion of iridium at high temperatures, J. Appl. Phys. 43 (1972) 2519–2521, https://doi.org/10.1063/1.1661553.
[31] J.K. Baria, The effect of temperature on lattice mechanical properties of noble and transition metals, Czech. J. Phys. 54 (2003) 575–595, https://doi.org/10.1023/B:CJOP.0000024960.14537.dd.
[32] C.P. Liang, G.H. Li, H.R. Gong, Concerning the brittleness of iridium: an elastic and electronic view, Mater. Chem. Phys. 133 (2012) 140–143, https://doi.org/10.1016/j.matchemphys.2011.12.080.
[33] L.V. Al'tshuller, A.A. Bakanova, Electronic structure and compressibility of metals at high pressures, Sov. Phys. Usp. 11 (1969) 678–689, https://doi.org/10.1070/PU1969v011n05ABEH003741.
[34] R.G. McQueen, S.P. Marsh, J.W. Taylor, J.N. Fritz, W.J. Carter, The Equation of State of Solids from Shock Wave Studies, High Velocity Impact Phenomena, Academic Press1970, pp. 293-417.
[35] S.P. Marsh, LASL Shock Hugoniot Data, University of California Press1980.
[36] J. Akella, High-pressure studies on iridium to 30.0 GPa, J. Phys. Chem. Solid. 43 (1982) 941, https://doi.org/10.1016/0022-3697(82)90045-2.
[37] V.V. Nemoshkalenko, V.Y. Mil'man, A.V. Zhalko-Titarenko, V.N. Antonov, Y. L. Shitikov, Dynamics of the iridium lattice:experiment and calculation, JETP Lett. 47 (1988) 295–298.
[38] H. Cynn, J.E. Klepeis, C.-S. Yoo, D.A. Young, Osmium has the lowest experimentally determined compressibility, Phys. Rev. Lett. 88 (2002) 135701, https://doi.org/10.1103/PhysRevLett.88.135701.
[39] H. Fang, L. Liu, M. Gu, S. Huang, C. Ni, Z. Li, R. Wang, High-pressure lattice dynamic and thermodynamic properties of Ir by first-principles calculation, Physica B 405 (2010) 732–737, https://doi.org/10.1016/j.physb.2009.09.096.
[40] P. Kumar, N.K. Bhatt, P.R. Vyas, V.B. Gohel, Thermophysical properties of iridium at finite temperature, Chin. Phys. B 25 (2016) 116401, https://doi.org/10.1088/1674-1056/25/11/116401.
[41] V. Monteseguro, J.A. Sans, V. Cuartero, F. Cova, I.A. Abrikosov, W. Olovsson, C. Popescu, S. Pascarelli, G. Garbarino, H.J.M. Jönsson, T. Irifune, D. Errandonea, Phase stability and electronic structure of iridium metal at the megabar range, Sci. Rep. 9 (2019), https://doi.org/10.1038/s41598-019-45401-x.
[42] C.T. Seagle, W.D. Reinhart, C.S. Alexander, J. Brown, J.-P. Davis, Shock Compression of Iridium, 2019. United States.
[43] K.V. Yusenko, S. Khandarkhaeva, T. Fedotenko, A. Pakhomova, S.A. Gromilov, L. Dubrovinsky, N. Dubrovinskaya, Equations of state of rhodium, iridium and their alloys up to 70 GPa, J. Alloys Compd. 788 (2019) 212–218, https://doi.org/10.1016/j.jallcom.2019.02.206.
[44] S. Anzellini, L. Burakovsky, R. Turnbull, E. Bandiello, D. Errandonea, P–V–T equation of state of iridium up to 80 GPa and 3100 K, Crystals 11 (2021) 452, https://doi.org/10.3390/cryst11040452.
[45] J. Han, L.-Q. Shi, N. Wang, H.-F. Zhang, S.-M. Peng, Equation of state of iridium: from insight of ensemble theory, J. Phys. Condens. Matter 34 (2022) 465702, https://doi.org/10.1088/1361-648X/ac93dc.
[46] N.A. Smirnov, Ab initio calculations of structural stability, thermodynamic and elastic properties of Ni, Pd, Rh, and Ir at high pressures, J. Appl. Phys. 134 (2023) 025901, https://doi.org/10.1063/5.0158737.
[47] K.V. Yusenko, E. Bykova, M. Bykov, S.A. Gromilov, A.V. Kurnosov, C. Prescher, V. B. Prakapenka, W.A. Crichton, M. Hanfland, S. Margadonna, L.S. Dubrovinsky, High-pressure high-temperature stability of *hcp*-Ir_xOs_{1-x}(x=0.50 and 0.55) alloys,

J. Alloys Compd. 700 (2017) 198–207, https://doi.org/10.1016/j.jallcom.2016.12.207.
[48] R.E. MacFarlane, J.A. Rayne, C.K. Jones, Temperature dependence of elastic moduli of iridium, Phys. Lett. 20 (1966) 234–235, https://doi.org/10.1016/0031-9163(66)90340-4.
[49] J.K. Baria, Temperature dependent lattice mechanical properties of some fcc transition metals, Chin. J. Phys. 42 (2004) 287–306.
[50] S. Kamran, K. Chen, L. Chen, Ab initio examination of ductility features of fcc metals, Phys. Rev. B 79 (2009), https://doi.org/10.1103/physrevb.79.024106.
[51] T. Ishikawa, P.-F. Paradis, R. Fujii, Y. Saita, S. Yoda, Thermophysical property measurements of liquid and supercooled iridium by containerless methods, Int. J. Thermophys. 26 (2004) 893–904, https://doi.org/10.1007/s10765-005-5585-3.
[52] T. Ishikawa, P.-F. Paradis, T. Itami, S. Yoda, Non-contact thermophysical property measurements of refractory metals using an electrostatic levitator, Meas. Sci. Technol. 16 (2005) 443, https://doi.org/10.1088/0957-0233/16/2/016.
[53] J.-W. Arblaster, Selected values for the densities and molar volumes of the liquid platinum group metals and of the initial melting curves of iridium, rhodium and ruthenium, Johnson Matthey Technol. Rev. 61 (2017) 81–87, https://doi.org/10.1595/205651317X694461.
[54] M. Leitner, G. Pottlacher, Density of liquid iridium and rhenium from melting up to the critical point, Int. J. Thermophys. 41 (2020) 139, https://doi.org/10.1007/s10765-020-02709-5.
[55] L. Wang, Y.C. Cho, Y.-H. Lee, J.J. Lee, G.W. Lee, Density measurement and uncertainty evaluation of elemental and alloy liquids using electrostatic levitation, J. Mol. Liq. 396 (2024) 123979, https://doi.org/10.1016/j.molliq.2024.123979.
[56] L. Burakovsky, N. Burakovsky, M.J. Cawkwell, D.L. Preston, D. Errandonea, S. I. Simak, Ab initio phase diagram of iridium, Phys. Rev. B 94 (2016) 094112, https://doi.org/10.1103/PhysRevB.94.094112.
[57] H. Okamoto, Suplemental literature review of binary phase diagrams: Ag-Ho, Ag-Tb, Ag-Y, Cd-Na, Ce-Sn, Co-Dy, Cu-Dy, Cu-Sn, Ir-Pt, Mg-Pb, Mo-Ni, and Sc-Y, J. Phase Equilibria Diffus. 35 (2014) 208–219, https://doi.org/10.1007/s11669-014-0284-z.
[58] A.V. Zadesenets, Y.V. Shubin, S.V. Korenev, Experimental investigation of phase equilibria of the Ir-Pt binary system in subsolidus region, Mater. Today Commun. 31 (2022) 103247, https://doi.org/10.1016/j.mtcomm.2022.103247.
[59] Y. Yamabe-Mitarai, T. Aoyagi, T. Abe, An investigation of phase separation in the Ir–Pt binary system, J. Alloys Compd. 484 (2009) 327–334, https://doi.org/10.1016/j.jallcom.2009.04.105.
[60] S.N. Tripathi, Thermodynamics properties of binary alloys of platinum metals II : Ir-Pt system, J. Less Common. Met. 91 (1983) 251–260, https://doi.org/10.1016/0022-5088(83)90319-3.
[61] E. Raub, Metals and alloys of the platinum group, J. Less Common. Met. 1 (1959) 3–18.
[62] L. Müller, Bestimmung der Schmelzpunkte von Slatinlegierungen, Ann. Phys. 399 (1930) 9–47, https://doi.org/10.1002/andp.19303990104.
[63] H. Okamoto, The Ir-Os (iridium-osmium) system, J. Phase Equil. 15 (1994) 55–57, https://doi.org/10.1007/BF02667683.
[64] T.H. Geballe, B.T. Matthias, V.B. Compton, E. Corenzwit, G.W. Hull, Superconductivity of solid solutions of noble metals, Phys. Rev. 129 (1963) 182–183, https://doi.org/10.1103/PhysRev.129.182.
[65] R.D. Reiswig, J.M. Dickinson, The osmium-iridium equilibrium diagram, Trans. Metall. Soc. AIME 240 (1964) 469–472.
[66] H.C. Vacher, C.J. Bechtoldt, E. Maxwell, Structure of some iridium-osmium alloys, JOM 6 (1954), https://doi.org/10.1007/BF03397984, 80-80.
[67] I.V. Korolkov, S.A. Gromilov, K.V. Yusenko, I.A. Baidina, S.V. Korenev, Crystal structure of [Ir(NH3)5Cl]2[OsCl6]Cl2. Crystal-chemical analysis of the iridium-osmium system, J. Struct. Chem. 46 (2005) 1052–1059, https://doi.org/10.1007/s10947-006-0241-8.
[68] P.S. Rudman, Lattice parameters of some h.c.p. binary alloys of rhenium and osmium: Re-W, Re-Ir, Re-Pt; Os-Ir, Os-Pt, J. Less Common. Met. 12 (1967) 79–81, https://doi.org/10.1016/0022-5088(67)90075-6.
[69] K.V. Yusenko, E. Bykova, M. Bykov, S.A. Gromilov, A.V. Kurnosov, C. Prescher, V. B. Prakapenka, W.A. Crichton, M. Hanfland, S. Margadonna, L.S. Dubrovinsky, High-pressure high-temperature stability of hcp-IrxOs1−x (x = 0.50 and 0.55) alloys, J. Alloys Compd. 700 (2017) 198–207, https://doi.org/10.1016/j.jallcom.2016.12.207.
[70] K.V. Yusenko, E. Bykova, M. Bykov, S.A. Gromilov, A.V. Kurnosov, C. Prescher, V. B. Prakapenka, M. Hanfland, S. van Smaalen, S. Margadonna, L.S. Dubrovinsky, Compressibility of Ir–Os alloys under high pressure, J. Alloys Compd. 622 (2015) 155–161, https://doi.org/10.1016/j.jallcom.2014.09.210.
[71] K.V. Yusenko, S.A. Martynova, S. Khandarkhaeva, T. Fedotenko, K. Glazyrin, E. Koemets, M. Bykov, M. Hanfland, K. Siemensmeyer, A. Smekhova, S. A. Gromilov, L.S. Dubrovinsky, High compressibility of synthetic analogous of binary iridium–ruthenium and ternary iridium–osmium–ruthenium minerals, Materialia 14 (2020) 100920, https://doi.org/10.1016/j.mtla.2020.100920.
[72] J.W. Arblaster, Selected values for the densities and molar volumes for the platinum group metals and of the initial melting curves of iridium, rhodium and ruthenium, Johnson Matthey Technol. Rev. 61 (2017) 81–87, https://doi.org/10.1595/205651317X694461.
[73] E. Raub, Metals and alloys of the platinum group, J. Less Common. Met. 1 (1959) 3–18, https://doi.org/10.1016/0022-5088(59)90014-1.
[74] E. Selbach, Electrical resistivity and lattice parameters of sputtered iridium alloys, Thin Solid Films 149 (1987) 17–28, https://doi.org/10.1016/0040-6090(87)90245-8.
[75] K.V. Yusenko, Personal Communication.